PCCP

COMMUNICATION

View Article Online
View Journal | View Issue

Cite this: *Phys. Chem. Chem. Phys.*, 2016, **18**, 29681

Received 21st June 2016,
Accepted 13th October 2016

DOI: 10.1039/c6cp04337b

www.rsc.org/pccp

On the origin of the great rigidity of self-assembled diphenylalanine nanotubes

Pavel Zelenovskiy,*[a] Igor Kornev,[b] Semen Vasilev[a] and Andrei Kholkin[ac]

The elastic properties of the nanotubes of self-assembled aromatic dipeptide diphenylalanine are investigated by means of Raman spectroscopy and a mass-in-mass 1D model. Analysis of nanotubes' lattice vibrations reveals the essential contribution of the water in the nanochannel core of the tubes to the Young's modulus and high water mobility along the channel. Direct measurements of the Young's modulus performed by nanoindentation confirm the obtained results.

Self-assembly of bioorganic materials is a convenient tool for the fabrication of functional micro- and nanodevices with outstanding properties.[1] Peptides are of particular importance as molecular building blocks because of their unique characteristics that can be tuned by changing the amino acid sequence and conjugating chemical groups to achieve better functionality.[2,3] Assembly mechanisms based on various noncovalent intermolecular interactions[4] allow peptides to readily adopt diverse 3D architectures such as vesicles, micelles, monolayers, bilayers, fibers, tubes, ribbons, spheres, and tapes.[5–7]

Recently, nanotubes of short aromatic peptides (namely, diphenylalanine, FF, consisting of two molecules of amino acid phenylalanine, F) have attracted significant attention, due to their outstanding physical and chemical properties, which are interesting from both the fundamental and applied points of view.[4–8] Along with inherent biocompatibility, they possess high aspect ratios,[9] strong piezoelectricity,[10,11] ferroelectricity,[12,13] and interesting optical properties related to quantum confinement of electrons and holes.[8,14] These useful functional properties are considered to be important for the design of novel biosensors and bioelectronic and biomolecular devices.[7,8] For example, it has been shown that microtubes of FF (self-assembled bundles of the nanotubes) exhibit clear piezoelectric resonance at MHz frequencies with high enough quality factor and can thus serve as piezoelectric sensors and actuators in micromechanical systems (MEMS).[10,15,16]

Special attention was paid to the remarkably rigid structure of FF nanotubes. Its experimentally measured transversal Young's modulus varies from 19 to 27 GPa,[17,18] and is several times larger than that of other peptide fibrils (about 3.3 GPa[19]). An attempt to shed light on the origin of such enormous stiffness was made using first-principles calculations.[20] However, the obtained value of the Young's modulus was still less than a half of the experimentally observed one, even when using the Tkatchenko–Scheffler (TS) correction, which allowed describing accurately hydrogen and van der Waals bonding, essential for biomolecular crystals.[20]

In our opinion, the main reason for such divergence is neglecting the water in the nanochannel core of the nanotubes. Its presence there was confirmed by X-ray analysis,[21] photoluminescence,[22] and Raman measurements.[23,24] Typically, FF nanotubes are produced from water rich solution, and water plays a crucial role in the nanotube formation.[25–27] Each FF monomer creates hydrogen bonds with water molecules,[21] which may thus contribute to the mechanical properties of the nanotubes. Exceptionally high values of Young's moduli (up to 44 GPa) due to hydrogen bonds between molecules were observed in several amino acid crystals.[28] A similar effect should be expected for the FF nanotubes.

In this work we developed a simple mechanical model of FF nanotubes taking into account the existence of water in the nanochannel core of the tubes. Analysis of nanotubes' lattice vibrations by Raman spectroscopy in the context of the proposed model allowed us to calculate effective elastic constants and to demonstrate the large contribution of water to the tubes' Young's moduli.

It is known that FF monomers in water-rich solution form helical nanotubes filled with water molecules *via* a self-assembly process.[21,23] Water molecules are held in the nanochannel core by radially oriented hydrogen bonds with FF monomers, whereas the latter interact among themselves *via* both hydrogen bonds and van der Waals forces.[21,29]

The unit cell of the nanotube (one step of the helix) consists of two embedded interacting subsystems: an FF ring (6 monomers)

[a] *Institute of Natural Sciences and Mathematics, Ural Federal University, Ekaterinburg, 620000, Russia. E-mail: zelenovskiy@urfu.ru*
[b] *SPMS Laboratory, Ecole Centrale Paris, Chatenay-Malabry, 92295, France*
[c] *Physics Department & CICECO – Aveiro Institute of Materials, University of Aveiro, Aveiro, 3810-193, Portugal*

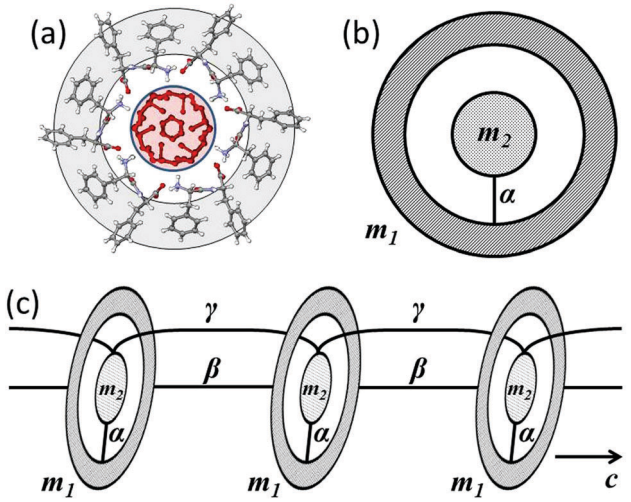

Fig. 1 The equivalent scheme of FF nanotubes. (a) Typical unit cell of an FF nanotube; (b) its mass-in-mass representation; and (c) nanotube formed by aligned interacting mass-in-mass units. Solid lines show interactions with spring constants α, β and γ. The arrow shows the tube's axis direction.

and water (24 molecules, 4 molecules per FF monomer[22]) inside the ring (Fig. 1(a)). Such systems can be described by the equivalent mass-in-mass unit of the same size (Fig. 1(b)). The masses of the FF ring and of its water "core" are $m_1 = 3.11 \times 10^{-24}$ kg and $m_2 = 0.72 \times 10^{-24}$ kg, respectively. Interaction between the FF ring and the water subsystem for the X and Y directions is characterized by the same effective spring constant α. The sequence of aligned unit cells forms the nanotube (Fig. 1(c)). Longitudinal interaction between adjacent rings and water therein occurs with effective spring constants β and γ, respectively. Individual nanotubes bond together by aromatic rings and form microtubes, which can be considered as a hexagonal crystal.[23,29]

The equations of motion for this system provide dispersive relations in the general form:

$$\omega^2 = \frac{\alpha}{2}\lambda(ka)\left\{1 \pm \sqrt{1 - 4\frac{f(ka)g(ka) - 1}{\mu M \lambda(ka)^2}}\right\}, \qquad (1)$$

where $\mu^{-1} = m_1^{-1} + m_2^{-1}$ – reduced mass, $M = m_1 + m_2$ – total mass of the unit cell, $f(ka) = 1 + 2(\beta/\alpha)[1 - \cos(ka)]$, $g(ka) = 1 + 2(\gamma/\alpha)[1 - \cos(ka)]$ and $\lambda(ka) = (f(ka)m_2 + g(ka)m_1)/(m_1 m_2)$. The sign in front of the square root corresponds to optical (+) or acoustical (−) branches.

It is worth noting that for $k = 0$ eqn (1) is reduced to a simple expression for vibrations of crystal with two atoms per primitive cell.[30] Therefore, keeping in mind the application to Raman scattering, the frequency of the optical mode at the center of the Brillouin zone is:[30]

$$\omega_{\text{opt}}(k = 0) = \sqrt{\frac{\alpha}{\mu}}. \qquad (2)$$

This expression can be used for determination of the spring constant α, assuming ω_{opt} to be an effective frequency of lattice vibrations measured by Raman spectroscopy. The obtained result will depend on the polarization conditions of the measurements, and therefore different spring constants α_{ij} relating to lattice vibrations in different directions in the nanotube can be obtained.

The effective elastic constants of FF nanotubes can be derived from the analysis of the Raman spectra. A comparison of the frequencies of acoustic vibrations obtained in the context of the used model with those calculated in continuous approximation gives a relation between microscopic spring constants α_{ij} and macroscopic elastic constants C_{ij}:[30]

$$C_{ij} = \frac{1}{2}\frac{\alpha_{ij} a_i a_j}{V}, \qquad (3)$$

where a_i is a corresponding lattice parameter (either a or c) and V is the cell volume (lattice parameters for the nanotube are:[21] $a = 24.1$ Å and $c = 5.46$ Å; therefore $V = \sin(\pi/3)a^2c = 2718.47$ Å^3).

For hexagonal crystals, the elastic constants form a tensor with five independent components (Voigt notations are used):[31] C_{11}, C_{12}, C_{13}, C_{33} and C_{44}. In the most common backscattering geometry of Raman measurements, a variation of the polarization direction allows determination of 4 components of the effective elastic tensor (Fig. 2). For $\bar{X}(zz)X$ and $\bar{X}(yy)X$ geometries, where polarization of a laser beam is parallel to the analyzer's orientation and is oriented either along or perpendicular to the tube axis, eqn (2) and (3) provide C_{33} and C_{11} constants, respectively. In the $\bar{X}(zy)X$ geometry the polarizations of the laser beam and the analyzer are 90°-crossed; therefore the constant C_{13} can be found. For estimation of the C_{12} constant the spectrum has to be measured on the end face of the tube in the $\bar{Z}(yx)Z$ geometry. The C_{44} constant cannot be determined by Raman spectroscopy. Raman spectra of all four geometries are presented in Fig. 3.

For estimation of effective elastic constants we used sufficiently long FF microtubes grown from water rich solution using a common procedure.[9,25] Raman spectra were measured using the confocal Raman microscope Alpha300AR (WITec GmbH, Germany)

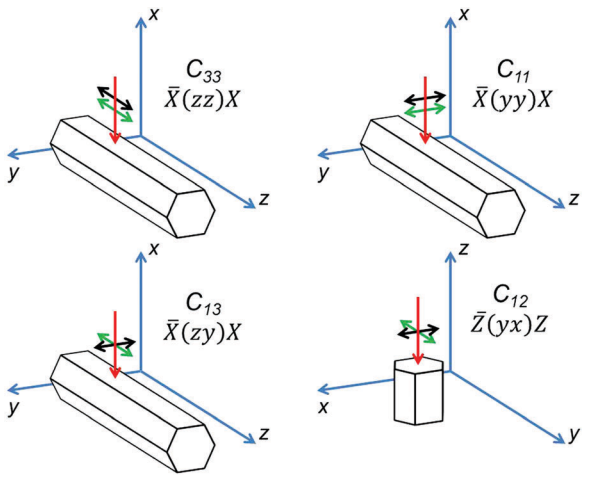

Fig. 2 Schemes of polarization directions for determination of the components of the effective elastic tensor in backscattering Raman measurements. Red arrow – direction of laser propagation, green arrow – laser polarization, and black arrow – polarization of analyzed light.

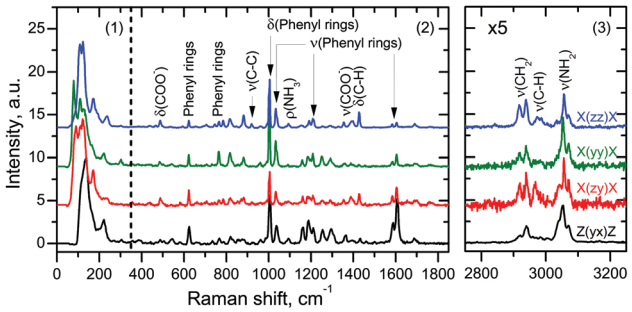

Fig. 3 Polarized Raman spectra of FF nanotubes in various geometries. Three characteristic regions: (1) lattice vibrations, and (2) and (3) vibrations of various functional groups. Attribution of several spectral lines to functional group vibrations is presented.

with an excitation wavelength of 488 nm and a spectral resolution of about 3 cm^{-1}.

A typical Raman spectrum of FF microtubes consists of three separate regions: region 1 (from 10 to 375 cm^{-1}) corresponds to lattice vibrations, whereas region 2 (from 375 to 1850 cm^{-1}) and region 3 (from 2750 to 3250 cm^{-1}) are due to vibrations of various functional groups (Fig. 3). Assignment of high-frequency spectral lines can be based on the analysis of published data,[32] whereas detailed analysis of low-frequency lines is hampered by a rather complicated tube structure and highly overlapping spectral lines. Deconvolution of this region into separate lines provides little information about the tube structure, regardless of the fact that the assignment of several low-frequency lines has been performed recently.[24]

The effective frequency of lattice vibrations can be calculated either by fitting the low-frequency spectral region by a single curve (Lorentzian or Gaussian) or by calculating the weighted average over this region. The second method is more precise since it takes into account low intensive lines, whereas fitting by a single curve mainly gives the maximum frequency in the region.

The calculation of the weighted average over the low-frequency region of Raman spectra (Fig. 3) gives average values of the effective frequency 131.2 and 126.8 cm^{-1} for $\bar{X}(zz)X$ and $\bar{X}(yy)X$ geometries, respectively, and 134.8 and 141.9 cm^{-1} for $\bar{X}(zy)X$ and $\bar{Z}(yx)Z$ geometries, respectively.

It is worth noting that edge filters, which are usually used in spectroscopic systems, cut part of the low-frequency region up to 50–100 cm^{-1}. However, this region is usually overlapped with a broad boson peak and shoulders of the Rayleigh line, and therefore information about the lattice vibrations here cannot be extracted anyway. We found that the spectral resolution of our instrument has little effect on the resulting elastic constants and even 30 cm^{-1} variation of the upper and lower limits of region 1 changes E_T and E_L by less than 0.3 GPa.

Thus, using the measured effective frequencies and estimated reduced mass of the ring, four independent components of effective elastic tensor C_{ij}^{W} of the water-filled nanotubes can be calculated. The obtained values are in line with those found in ref. 20 within a density functional theory calculation using the Perdew–Burke–Ernzerhof (PBE) generalized gradient approximation for the exchange–correlation (Table 1).

Table 1 Effective elastic constants of FF nanotubes (in GPa). Constants C_{ij}^{FF} describe interaction between FF monomers and are obtained in first-principles calculations in PBE and PBE+TS schemes.[20] Constants C_{ij}^{W} are calculated in this work and show the contribution of water molecules present in the core of the nanotubes. The total effective elastic constants are $C_{ij}^{tot} = C_{ij}^{W} + C_{ij}^{FF}$

	C_{ij}^{FF}		C_{ij}^{W}	C_{ij}^{tot}
	PBE	PBE+TS		
C_{11}	5.29	17.56	9.17	26.73
C_{12}	2.18	11.91	2.60	14.51
C_{13}	2.34	11.00	2.35	13.35
C_{33}	14.08	24.05	0.50	24.55

The values of C_{12} and C_{13} are close to those calculated in ref. 20 for empty tubes (Table 1), whereas a higher value of C_{11} demonstrates the pronounced effect of the water subsystem on the elasticity of the tube in a transversal direction. The low value of C_{33} shows that water molecules are weakly bound to FF rings and can easily move along the nanochannel, thus making FF tubes interesting for various micro- and nanofluidic applications.[33] At the same time, the longitudinal mobility of water has only a negligible effect on the longitudinal stiffness of the tube, which is therefore determined by the interaction between FF monomers in the adjacent rings only. This interaction cannot be taken into account in our model, since eqn (2) for the effective frequency of the lattice vibrations does not include the spring constant β.

To take into account both water and FF contributions, the total elastic constants of the FF nanotubes can be calculated: $C_{ij}^{tot} = C_{ij}^{W} + C_{ij}^{FF}$. Here C_{ij}^{W} describes water contribution and is found in this work in the context of the proposed model. For C_{ij}^{FF} we used elastic constants calculated in ref. 20 in the "PBE+TS" approach, *i.e.* with the van der Waals interactions after the Tkatchenko–Scheffler scheme included on top of the PBE exchange-correlation. The inclusion of this interaction is essential for accurately describing the long-range interaction between FF rings. The obtained values of the total elastic constants are presented in Table 1.

The hardness of the FF microtubes can be described by transversal E_T (across the tube) and longitudinal E_L (along the tube) Young's moduli due to the anisotropy of the microtubes. E_T and E_L can be written in terms of elastic constants:[34]

$$E_T = \frac{C_{11}^2 C_{33} + 2C_{13}^2 C_{12} - 2C_{11}C_{13}^2 - C_{33}C_{12}^2}{C_{11}C_{33} - C_{12}^2}, \quad (4)$$

$$E_L = \frac{C_{11}^2 C_{33} + 2C_{13}^2 C_{12} - 2C_{11}C_{13}^2 - C_{33}C_{12}^2}{C_{11}^2 - C_{12}^2}. \quad (5)$$

Total elastic constants C_{ij}^{tot} were used to calculate E_T (Table 2), which is noticeably greater than that obtained in first-principles calculations[20] and is very close to the experimentally derived value, 19 GPa.[18] This demonstrates that the water subsystem essentially contributes to the stiffness of the FF nanotubes in the transversal direction. This is, most probably, due to the radial network of hydrogen bonds between FF

Table 2 Young's moduli of FF nanotubes (in GPa)

	Calculations			Experiments	
	First-principles[a]		This work	AFM	This work
E_T	4.24	8.75	16.77	19[b]	10
				27 ± 4[c]	25
E_L	12.6	15.85	15.91	—	—

[a] Ref. 20. [b] Ref. 18. [c] Ref. 17.

monomers in the ring and water molecules. This effect is similar to that observed in several amino acid crystals.[28]

However, the obtained value (16.77 GPa) is far though from another experimental value (27 GPa).[17] This experimental value was obtained by a bending beam model using an atomic force microscope (AFM) on nanotubes suspended across the micro-cavities. However, this method provides results strongly depending on the nanotube fixed at the edges of the cavity.[35,36]

To get more precise values of the transversal Young's modulus, we performed direct measurements of E_T by the dynamical nanoindentation method. The nano-hardness tester NanoScan-4D (FSBI TISNCM, Russia) equipped with a Berkovich indenter (diamond pyramid) was used. The values of E_T were determined from loading–unloading curves by the Oliver–Pharr method.[37] Measurements were performed in more than 50 points of several FF nanotubes fixed at the solid substrate. Our tests showed an instrumental error less than 2%.

Two characteristic values of E_T were revealed (see Table 2 and Fig. 4). The first value (10 GPa) is close to that obtained from first-principles modeling of empty nanotubes.[20] The second value (25 GPa) is close to that measured in ref. 17. The dispersion of these characteristic values is larger than the instrumental error, reproducible and can be attributed to inhomogeneous filling of the nanotubes due to the high mobility of water molecules along the nanochannel.[38,39] In this case the lowest values of the Young's modulus correspond to almost empty nanotubes, whereas completely filled tubes provide the largest E_T (see insets in Fig. 4). It is worth noting that only a part of the water molecules in FF tubes is considered in our model. This corresponds to partially filled nanotubes, and therefore the value of E_T calculated in the present work falls into the intermediate range (Fig. 4). Additional water molecules that can exist in the nanochannel core[40,41] introduce additional stiffness into the nanotube, and therefore higher values of Young's moduli can be observed. The highest observed value of E_T is about 31 GPa (Fig. 4).

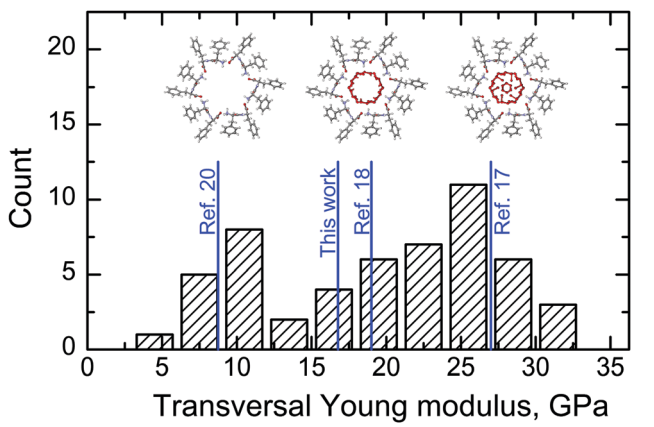

Fig. 4 Values of E_T measured directly by the nanoindentation method. The inset shows FF nanotubes with different degrees of filling by water: empty nanotubes, partially filled nanotubes, and completely filled nanotubes. Blue solid lines point out values obtained from the literature and calculated in this work.

Finally, the value of E_L calculated in this work is very close to that obtained in ref. 20 in PBE–TS approximation, since movable water molecules weakly contribute to longitudinal stiffness. Experimental measurements of this value are conjugated with high technical difficulties and are still to be done.

In summary, the essential contribution of water molecules inside the nanochannel of diphenylalanine peptide nanotubes to its transversal Young's modulus is demonstrated. Analysis of the low-frequency region of the Raman spectra of the nanotubes in the context of a mass-in-mass 1D model allowed refining four independent constants in the effective elastic tensor and to demonstrate the high mobility of water molecules along the nanochannels. Direct measurements of the transversal Young's modulus using a nanoindenter showed that its value strongly depends on the degree of nanotube filling by water, whereas the longitudinal Young's modulus is primarily determined by the interaction between peptide monomers.

The equipment of the Ural Center for Shared Use "Modern nanotechnology" UrFU was used. The research was made possible by the President of Russian Federation grant for young scientists (Contract 14.Y30.15.6554-MK), by the Government of the Russian Federation (Act 211, Agreement 02.A03.21.0006), and by the Ministry of Foreign Affairs of France within Metchnikov Scholarship (grant 851365A). Part of this work was developed in the scope of Project CICECO-Aveiro Institute of Materials (ref. FCT UID/CTM/50011/2013), financed by national funds through the FCT/MEC and, when applicable, cofinanced by FEDER under the PT2020 Partnership Agreement.

References

1 J.-M. Lehn, *Science*, 2002, **295**, 2400–2403.
2 C.-L. Chen and N. Rosi, *Angew. Chem., Int. Ed.*, 2010, **49**, 1924–1942.
3 C. A. E. Hauser and S. Zhang, *Chem. Soc. Rev.*, 2010, **39**, 2780–2790.
4 S. Cavalli, F. Albericio and A. Kros, *Chem. Soc. Rev.*, 2010, **39**, 241–263.
5 E. Gazit, *Chem. Soc. Rev.*, 2007, **36**, 1263–1269.
6 G. Rosenman, P. Beker, I. Koren, M. Yevnin, B. Bank-Srour, E. Mishina and S. Semin, *J. Pept. Sci.*, 2011, **17**, 75–87.
7 L. Adler-Abramovich and E. Gazit, *Chem. Soc. Rev.*, 2014, **43**, 6881–6893.
8 D. Bonetti, A. Toto, R. Giri, A. Morrone, D. Sanfelice, A. Pastore, P. Temussi, S. Gianni and M. Brunori, *Phys. Chem. Chem. Phys.*, 2014, **16**, 6391–6397.
9 A. Nuraeva, S. Vasilev, D. Vasileva, P. Zelenovskiy, D. Chezganov, A. Esin, S. Kopyl, K. Romanyuk, V. Y. Shur and A. L. Kholkin, *Cryst. Growth Des.*, 2016, **16**, 1472–1479.

10 A. Kholkin, N. Amdursky, I. Bdikin, E. Gazit and G. Rosenman, *ACS Nano*, 2010, **4**, 610–614.
11 S. Vasilev, P. Zelenovskiy, D. Vasileva, A. Nuraeva, V. Y. Shur and A. L. Kholkin, *J. Phys. Chem. Solids*, 2016, **93**, 68–72.
12 Z. Gan, X. Wu, X. Zhu and J. Shen, *Angew. Chem., Int. Ed.*, 2013, **52**, 2055–2059.
13 I. Bdikin, V. Bystrov, S. Kopyl, R. P. G. Lopes, I. Delgadillo, J. Gracio, E. Mishina, A. Sigov and A. L. Kholkin, *Appl. Phys. Lett.*, 2012, **100**, 043702.
14 N. Amdursky, M. Molotskii, D. Aronov, L. Adler-Abramovich, E. Gazit and G. Rosenman, *Nano Lett.*, 2009, **9**, 3111–3115.
15 R. de la Rica, C. Pejoux and H. Matsui, *Adv. Funct. Mater.*, 2011, **21**, 1018–1026.
16 E. D. Bosne, A. Heredia, S. Kopyl, D. V. Karpinsky, A. G. Pinto and A. L. Kholkin, *Appl. Phys. Lett.*, 2013, **102**, 073504.
17 L. Niu, X. Chen, S. Allen and S. J. B. Tendler, *Langmuir*, 2007, **23**, 7443–7446.
18 N. Kol, L. Adler-Abramovich, D. Barlam, R. Z. Shneck, E. Gazit and I. Rousso, *Nano Lett.*, 2005, **5**, 1343–1346.
19 J. F. Smith, T. P. J. Knowles, C. M. Dobson, C. E. MacPhee and M. E. Welland, *Proc. Natl. Acad. Sci. U. S. A.*, 2006, **103**, 15806–15811.
20 I. Azuri, L. Adler-Abramovich, E. Gazit, O. Hod and L. Kronik, *J. Am. Chem. Soc.*, 2014, **136**, 963–969.
21 J. Kim, T. H. Han, Y.-I. Kim, J. S. Park, J. Choi, D. G. Churchill, S. O. Kim and H. Ihee, *Adv. Mater.*, 2010, **22**, 583–587.
22 M. Wang, S. Xiong, X. Wu and P. K. Chu, *Small*, 2011, **7**, 2801–2807.
23 X. Wu, S. Xiong, M. Wang, J. Shen and P. K. Chu, *J. Phys. Chem. C*, 2012, **116**, 9793–9799.
24 X. Wu, S. Xiong, M. Wang, J. Shen and P. K. Chu, *Opt. Express*, 2012, **20**, 5119–5126.
25 P. S. Zelenovskiy, V. Y. Shur, A. S. Nuraeva, S. G. Vasilev, D. S. Vasileva, D. O. Alikin, D. S. Chezganov, V. P. Krasnov and A. L. Kholkin, *Ferroelectrics*, 2015, **475**, 127–134.
26 M. I. Souza, E. R. Silva, Y. M. Jaques, F. F. Ferreira, E. E. Fileti and W. A. Alves, *J. Pept. Sci.*, 2014, **20**, 554–562.
27 T. D. Do and M. T. Bowers, *Anal. Chem.*, 2015, **87**, 4245–4252.
28 I. Azuri, E. Meirzadeh, D. Ehre, S. R. Cohen, A. M. Rappe, M. Lahav, I. Lubomirsky and L. Kronik, *Angew. Chem., Int. Ed.*, 2015, **54**, 13566–13570.
29 C. H. Gorbitz, *Chem. Commun.*, 2006, 2332–2334.
30 C. Kittel, *Introduction to Solid State Physics*, John Wiley & Sons, New York, 1953.
31 J. F. Nye, *Physical Properties of Crystals: Their Representation by Tensors and Matrices*, Oxford University Press, Oxford, NY, 1957.
32 B. Hernandez, F. Pfluger, S. G. Kruglik and M. Ghomi, *J. Raman Spectrosc.*, 2013, **44**, 827–833.
33 N. B. Sopher, Z. R. Abrams, M. Reches, E. Gazit and Y. Hanein, *J. Micromech. Microeng.*, 2007, **17**, 2360.
34 A. F. Bower, *Applied Mechanics of Solids*, CRC Press, Boca Raton, FL, 2009.
35 Y. Chen, B. L. Dorgan, D. N. McIlroy and E. D. Aston, *J. Appl. Phys.*, 2006, **100**, 104301.
36 D. Kluge, F. Abraham, S. Schmidt, H.-W. Schmidt and A. Fery, *Langmuir*, 2010, **26**, 3020.
37 W. Oliver and G. Pharr, *J. Mater. Res.*, 1992, **7**, 1564–1583.
38 J. Comer, F. Dehez, W. Cai and C. Chipot, *J. Phys. Chem. C*, 2013, **117**, 26797.
39 L. Ruiz, Y. Wu and S. Keten, *Nanoscale*, 2015, **7**, 121.
40 C. H. Gorbitz, *Chem. – Eur. J.*, 2001, **7**, 5153.
41 T. Andrade-Filho, T. C. Martins, F. F. Ferreira, W. A. Alves and A. R. Rocha, *Theor. Chem. Acc.*, 2016, **135**, 185.